Title: Feasibility and preliminary accuracy of high-resolution imaging of the liver and pancreas using FNA compatible microendoscopy

Authors: [1]Renu Regunathan, MD, [2]Jenny Woo, MD, [3]Mark C Pierce, PhD, [4]Alexandros D Polydorides, MD, PhD, [5]Mohammad Raoufi, MD, [2]Sasan Roayaie, MD, [2]Myron Schwartz, MD, [2]Daniel Labow, MD, [6]Dongsuk Shin, BS, [7]Rei Suzuki, MD, [7]Manoop S Bhutani, MD, [8]Lezlee G Coghlan, DVM, [6]Rebecca Richards-Kortum, PhD, [2]Sharmila Anandasabapathy, MD, [2]Michelle Kang Kim, MD, MSc

Current Affiliations:

1) Columbia University, Department of Medicine, New York NY
2) The Mount Sinai Medical Center, Department of Gastroenterology, New York NY
3) Rutgers, The State University of New Jersey, Department of Biomedical Engineering, Piscataway NJ
4) The Mount Sinai Medical Center, Department of Pathology, New York NY
5) Henry Ford Hospital, Department of Pathology, Detroit MI
6) Rice University, Department of Bioengineering, Houston TX
7) The University of Texas MD Anderson Cancer Center, Department of Gastroenterology, Hepatology and Nutrition, Houston, TX
8) The University of Texas MD Anderson Cancer Center, Science Park, Department of Molecular Carcinogenesis, Smithville, TX

Corresponding Author:

Michelle Kang Kim, MD, MSc
One Gustave Levy Place, Box 1069
New York, NY 10029
Phone: (212)241-7535
Fax: (212) 241-2276
Email: michelle.kim@mssm.edu

Abstract:

Background: Endoscopic ultrasound-guided fine needle aspiration (EUS-FNA) is one of the few techniques which can obtain cells and tissue from the liver and pancreas. However, the technique remains vulnerable to poor specimen quality and sampling error.

Objectives: To evaluate the ability of a high-resolution microendoscope (HRME) to visualize the cellular and architectural features of normal and malignant liver and pancreatic tissue *ex vivo*. To assess the ability of endosonographers to identify normal and neoplastic tissue using HRME images. To demonstrate preliminary technical feasibility of *in vivo* HRME imaging via EUS-fine needle puncture (FNP).

Design: *Ex vivo*, pilot feasibility study in human tissue; *in vivo* swine model.

Setting: Two academic medical centers

Patients and Interventions: Co-registered HRME images and biopsies were obtained from surgically resected hepatic and pancreatic tissues from a total of 44 patients. Images were divided into training (12 images) and test sets (80 images) containing a range of normal and pathologic conditions for each organ. After viewing the training sets, nine endosonographers attempted to distinguish malignant tissue from normal or benign lesions in the test sets, each of which contained 40 unique images with individual diagnoses from pathology.

Main Outcome Measurements: Image acquisition feasibility, *ex vivo* and *in vivo*. Ability of endosonographers to recognize features of normal/benign or malignant tissue from the liver and pancreas.

Results: Overall, the nine endosonographers achieved median accuracy figures of 85% in the liver and 90% in the pancreas. The endosonographers with prior experience in reading HRME images achieved accuracy rates between 90% and 95%. Technical feasibility of HRME imaging through a 19-gauge EUS-FNP needle was demonstrated in an *in vivo* swine model.

Limitations: *Ex vivo* study

Conclusions: High-resolution microendoscopy allows real-time imaging of cellular-level morphology and tissue architecture in the liver and pancreas. The techniques appears to have a short learning curve, after which endosonographers achieved high accuracy rates in distinguishing malignant tissue from normal and benign pathology in both organs. Translating this imaging platform to the *in vivo* setting appears technically feasible.

Introduction:

Endoscopic ultrasound (EUS) is commonly used to visualize intra-abdominal organs including the liver and pancreas, and in conjunction with fine needle aspiration (EUS-FNA) to sample tissue from these organs. In early studies, EUS-FNA was found to be equal or superior to other imaging modalities including CT and MRI for assessing tumor size and lymph node involvement[1]. However, EUS-FNA has been shown to have a failure rate of up to 10% due to poor specimen quality, sampling error, and its inability to distinguish confounders such as acute and chronic pancreatitis[2-5].

Background:

Several real-time adjunctive techniques are being developed to improve the diagnostic accuracy of EUS-FNA, including contrast enhancement, elastography, and confocal laser endomicroscopy[6-11]. However, due to factors including cost, complexity, and their associated learning curves, these methods have not yet gained widespread acceptance in clinical practice. We have recently developed a high-resolution microendoscope (HRME) which is a fiber-optic probe-based system which provides images of cellular morphology and tissue architecture *in situ* and in real-time (fig. 1a,b)[12,13]. This prototype device costs less than $2,500 in components, with a probe that can be passed though a 22-gauge needle and be sterilized and reused (fig. 1c). Previous *ex vivo* and *in vivo* studies in the esophagus and colon demonstrated the feasibility of obtaining high-resolution images of the epithelial mucosa using the HRME, aimed at providing targeted guidance for biopsy collection[14,15]. A recent study demonstrated the technical feasibility of performing confocal endomicroscopy in the pancreas *in vivo* via a 19-gauge FNA needle, with image quality described as "good to very good" in 10 out of 18 cases[16]. HRME imaging does not provide the optical sectioning ability of confocal endomicroscopy, but has nevertheless demonstrated very good image quality in other gastrointestinal organs *in vivo*, and is significantly less expensive than confocal platforms[15]. The aims of the study reported here were (1) to identify the characteristic features of normal tissue, benign lesions, and neoplasms in the liver and pancreas which are apparent under

HRME imaging, and (2) to estimate the accuracy and learning curve for endosonographers to identify malignant neoplasms in these organs using images obtained with the HRME.

Methods:

Under an IRB approved protocol, we obtained written informed consent from 32 patients undergoing liver resection and 12 undergoing pancreatic resection. The patient population comprised 25 women and 19 men, with a mean age of 60 years. Technical details of the HRME have been described in detail elsewhere[13]. Briefly, the device essentially operates as a fluorescence microscope, coupled to a fiber-optic imaging probe (fig. 1a,b). Following application of a fluorescent contrast agent, the probe is placed in contact with the tissue, with an image of the tissue site transmitted back through the fiber-optic probe and captured by a CCD camera. In common with previous studies by our group[14,15] and others in the GI literature[9,17] we used 0.01% w/v proflavine solution as the fluorescent contrast agent to label cell nuclei. The HRME system used here to image human tissues has 4.4 μm spatial resolution, a 0.72 mm diameter field of view, and displays images in real-time at 12 frames per second. Use of a probe with 0.33 mm field of view allows passage through a 22-gauge EUS-FNA needle (Cook ECHO-1-22) (fig. 1c).

Immediately following resection, each fresh tissue specimen was evaluated by a gastrointestinal pathologist who identified up to four normal and four neoplastic sites by gross examination. Proflavine was topically applied to the tissue surface and HRME images were immediately acquired by direct placement of the probe on the tissue surface at each designated site. A single application of contrast agent was typically sufficient for several minutes of imaging; no rinsing of excess dye was required. Sample sections from each imaged site were then placed in formalin and submitted for histopathologic processing. Each specimen was given a histologic diagnosis by an expert pathologist using standard criteria, blinded to the corresponding HRME image.

To assess the ability of endosonographers to identify malignant neoplasms on HRME, individual images were assigned to separate "training" or "test" data sets for both the liver and the pancreas. The training set for the liver contained seven unique HRME images from a range of biopsy-proven normal, benign, and malignant tissue sites. The training set for the pancreas contained five HRME images. All endosonographers viewed the same training and test images in the same order. Each test set comprised 40 unique images which were not included in the corresponding training set. Examples of hepatic pathology included lesions such as cholangiocarcinoma, angiomyolipoma, and metastatic colon cancer, with pancreatic pathology including such conditions as serous microcystic cystadenoma and ductal adenocarcinoma. Nine endosonographers from multiple regional academic institutions participated in this study, each having performed more than 1000 EUS cases. The endosonographers were blinded to all patient history for the purposes of the study and were not involved in the generation of the training and test image sets. After viewing the training sets and being informed of the characteristic image features of each tissue type, participants were asked to evaluate the test sets for the both organs and state whether each image represented normal, benign, or malignant tissue.

To evaluate the technical feasibility of performing *in vivo* HRME imaging in conjunction with EUS-FNP, experiments were performed in a swine model. All experiments were approved by the Institutional Animal Care and Use Committee (IACUC) at The University of Texas MD Anderson Cancer Center. Following administration of anesthesia, a linear echoendoscope (Olympus GFUC30P) was introduced into the stomach. The stomach wall was punctured with a 19-gauge EUS-FNA needle (Cook, ECHO-1-19) and advanced into the pancreatic parenchyma under EUS guidance. Following removal of the needle stylus, 5 ml of proflavine was injected through the needle. The HRME imaging fiber was then passed through the needle into the pancreas for imaging.

Results:

HRME Image Features:

Figure 2 shows HRME images and corresponding histopathology from the liver. On HRME imaging of normal hepatic tissue (fig. 2a), individual nuclei are bright, evenly spaced, regularly shaped, and round to oval. In the corresponding H&E stained section (fig. 2d), normal hepatocytes have small, regularly spaced and centrally located round nuclei. In the HRME image of a benign angiomyolipoma (fig. 2b), there are large dark spaces representing lipid vacuoles outlined by haphazardly arranged cells with small, well defined nuclei. The corresponding H&E section (fig. 2e) shows a mix of adipocytes with large vacuoles, among chronic inflammatory cells and well differentiated smooth muscle cells with discrete nuclei. Tissue at the site of a metastatic colon adenocarcinoma shows loss of normal hepatic architecture in both the HRME image (fig. 2c) and the H&E section (fig. 2f) with poorly formed, irregular glandular structures leading to apparent nuclear crowding and clumping.

In the normal pancreas, nuclei appear as clustered small bright dots in the HRME image (fig. 3a), while the H&E section reveals small nuclei grouped in well formed, regularly spaced round acinar structures (fig. 3d). In benign microcystic adenoma, large cystic spaces of variable shapes and sizes can be identified in both the HRME image (fig. 3b) and H&E section (fig. 3e). Real-time HRME imaging at this site is shown in accompanying Video Clip 1. In ductal adenocarcinoma, there is loss of normal architecture with irregular clumps of streaking nuclei in the HRME image (fig. 3c) and, correspondingly, small irregular glands infiltrating amidst a desmoplastic stroma in the H&E section (fig. 3f). No normal acini are seen.

The primary focus of this study was to establish the characteristic features of normal, benign, and malignant tissue in the liver and pancreas on HRME imaging, by using an *ex vivo* study with well correlated histopathology sections. To make an initial assessment of the technical feasibility of translating this imaging method to the *in vivo* setting, we performed a small series of experiments in an *in vivo* swine model, allowing us to assess factors including contrast agent delivery, intraparenchymal image quality, effect of blood in the field, and subject motion artifact. Figure 4 presents a representative HRME image from the swine pancreas, acquired *in vivo* using EUS-FNP. As with the normal *ex vivo* human pancreas, nuclei appear as discrete bright dots, regularly spaced throughout the HRME field-of-view. We found that delivery of the contrast agent was straightforward, and manipulation of the HRME probe was essentially comparable to working with the EUS-FNA device alone.

HRME image feature recognition and learning curve:

Two of the nine endosonographers who completed the test sets had previous experience in viewing and interpreting HRME images (> 50 cases each), while seven had no prior experience in using HRME or interpreting HRME images. For the group as a whole, the median accuracy for identifying malignant versus normal or benign tissue in the liver was 85%, with 81% sensitivity and 88% specificity. The median positive predictive value (PPV) and negative predictive value (NPV) for detection of malignant lesions of the liver were 81% and 87% respectively. In the pancreas, the median accuracy of the group for identification of malignant lesions was 90%, with sensitivity and specificity 85% and 90%, respectively. The PPV and NPV for identifying pancreatic malignancies were 90% and 86%. These data are presented in fig. 5a and for each individual endosonographer in Table 1.

The two endosonographers with prior experience in HRME were better at classifying images than those without, achieving accuracy figures of 90% in the liver and 95% for the pancreas, compared to median

values of 83% and 68% respectively for the "novice" group. The "HRME experienced" endosonographers achieved sensitivity and specificity figures of 91% and 90% respectively for identifying malignant sites in the liver, compared to 63% and 83% respectively for the "HRME novice" group (fig. 5b). In the pancreas, the "experienced" group achieved sensitivity and specificity of 95% and 95% respectively for detecting malignant lesions, compared to 75% and 85% for the "novice" group. When "normal" and "benign" categories were grouped for analysis, Cohen's kappa inter-rater reliability for the two "HRME experienced" endosonographers was 0.80 for both the liver and the pancreas. Fleiss' kappa for the group of seven "HRME novice" endosonographers was 0.39 for the liver and 0.27 for the pancreas. When all three categories (normal, benign, malignant) remained separate, Cohen's kappa for the experienced group was 0.70 for the liver and 0.84 for the pancreas. Fleiss' kappa for the novice group was 0.44 for the liver and 0.22 for the pancreas.

Discussion:

Several endoscopic techniques for evaluating tissue structure and cell-level morphology have been developed recently, the majority focusing on applications in the esophagus and colon[9,18-20]. A feasibility study demonstrating confocal endomicroscopy of the pancreas was recently reported, highlighting the potential for endomicroscopy to serve as an adjunct to EUS-FNA[16]. While histopathologic evaluation will remain the gold standard for diagnosis, the advantage of high-resolution endomicroscopy is that real biopsies can be performed in a more targeted manner, potentially increasing diagnostic accuracy. The ability to obtain real-time microscopic information during EUS-FNA would also be particularly helpful where on-site cytopathologic evaluation is not available. Despite these potential benefits, two key factors may influence the degree to which these technologies are adopted into clinical practice. The first concerns the accuracy of the technique and the associated learning curve for the anticipated users. A second factor which impacts the diffusion of any new technology is instrument cost. We began to address

these questions here by developing a low-cost instrument with a re-usable fiber-optic probe ($2,500 processor, $500 probe), and measuring the ability of endosonographers to differentiate neoplastic lesions in both the liver and pancreas.

Our group of 9 endosonographers identified malignant lesions of the liver and pancreas in 40-image test sets with a median accuracies of 85% and 90% respectively, despite the fact that 7 participants had no prior experience with microendoscopic imaging. The 2 experienced endosonographers with over 50 cases each involving HRME imaging achieved an average accuracy of 90% and 95% for the liver and pancreas, respectively, suggesting that interpretation of HRME images has a relatively short learning curve. A small number of studies have attempted to evaluate the learning curve for endomicroscopy in other organs. Buchner *et al.* found that users of probe-based confocal endomicroscopy were able to interpret images for identification of colorectal polyps with an accuracy of 93% after reading at least 35 cases[21]. However, it is difficult to compare post-training accuracy figures for different organ sites, and also for systems using different contrast agents which require recognition of different classification features. Nevertheless, it appears that confocal endomicroscopy and HRME may have similar learning curves, on the order of a few 10's of cases. In addition to this purely qualitative interpretation of images, there is clearly scope for quantitative image analysis to measure morphological characteristics such as total number of nuclei per field, average nuclear size, and nuclear–to-cytoplasmic ratio. Values from the most diagnostically relevant parameters can be used to create an automated algorithm to provide an objective evaluation of tissue in real-time during the imaging process.

The primary limitation of this study was the use of *ex vivo* surgical specimens. Our feasibility experiments in an *in vivo* swine model permitted assessment of *in vivo* factors including motion artifacts and sampling error, and the impact of bleeding on image acquisition and interpretation. The experience

gained with this model suggests that *in vivo* deployment in humans is technically feasible. The current study design enabled us to use co-registered images and corresponding tissue sections to provide an accurate pathologic diagnosis as the gold-standard, which was not the case in the *in vivo* study reported by Konda *et al.* [16]. We characterized image features in normal, benign, and malignant tissues of both the liver and pancreas, and assembled nine endosonographers with varying levels of experience to establish both the accuracy and estimated learning curve for HRME. Recognition of benign conditions including angiolipoma and serous microcystic adenoma could be more difficult in practice, due to the fact that characteristic voids in the nuclear staining pattern on HRME could also arise from other disorders, both benign and malignant, such as angiosarcoma, peliosis hepatitis and NASH. An additional limitation was related to the availability of multiple tissue specimens with a wider range of pathology, such as intraparenchymal sites, which would have enabled us to train and test the endosonographers more comprehensively. A smaller fiber-probe with correspondingly reduced field-of-view will need to be used for passage through a 22-gauge EUS-FNA needle; however, the resolution (and therefore image quality) is not affected by the fiber diameter and is expected to be maintained at the level shown here.

In order to translate this technology into the patient setting several issues will need to be addressed. Delivery of the fluorescent contrast agent to the target organ prior to imaging could be performed by first delivering the dye through the EUS needle itself, followed by insertion of the HRME fiber. This was the approach we adopted for the *in vivo* swine imaging. Alternatively, Tanbakuchi *et al.* demonstrated a clinical confocal system with a contrast agent delivery channel mounted directly alongside the imaging fiber bundle[22]; such an approach could be adapted for HRME imaging within an EUS needle. These approaches could be applied to topical agents, however, as reported by other groups in the confocal endomicroscopy literature[16,23], intravital imaging dyes such as fluoroscein or indocyanine green can be delivered by an intravenous route. The fluorescent dye used here (proflavine) has been used by our group and others for several clinical endomicroscopy studies[9,15,17], however it does not currently have full FDA

approval as an imaging agent. Our experience with proflavine, used under Investigational New Drug (IND) status in the esophagus and colon since 2009 has not resulted in any adverse events and we are continuing to monitor subjects enrolled in these studies.

A second intriguing question for future clinical use is how to best integrate image information from high-resolution microendoscopy with that from the EUS imaging modality. It seems likely that the endosonographer would wish to integrate macroscopic information from EUS with the microscopic scale information from HRME, and future prospective study of EUS/FNA cases will be designed to take this into account.

In conclusion, we demonstrated that a novel, low-cost endomicrocopy device could be used to acquire high-quality, high-resolution images of cellular morphology and architecture in surgical specimens from the liver and pancreas. *In vivo* translation appears feasible based upon pilot animal data. With experience in HRME image interpretation, users achieved diagnostic accuracy rates of up to 95%. This innovative technique can potentially improve further upon EUS-FNA, increasing its diagnostic accuracy with minimal added cost and risk.

Acknowledgments:

This project was supported by award number U54CA143837 from the National Cancer Institute (NCI), by award number R01EB002179 from the National Institute of Biomedical Imaging and Bioengineering (NIBIB), and by The Cockrell Foundation. The content is solely the responsibility of the authors and does not necessarily represent the official views of the NCI, NIBIB, or the National Institutes of Health.

Figures:

Figure 1: The high-resolution microendoscope (HRME). (a) Schematic diagram. (b) Photograph of the HRME unit, measuring 10" x 8" x 2.5". (c) Photograph of fiber optic probe with 0.45 mm diameter passed through a EUS-FNA needle (Cook ECHO-1-22).

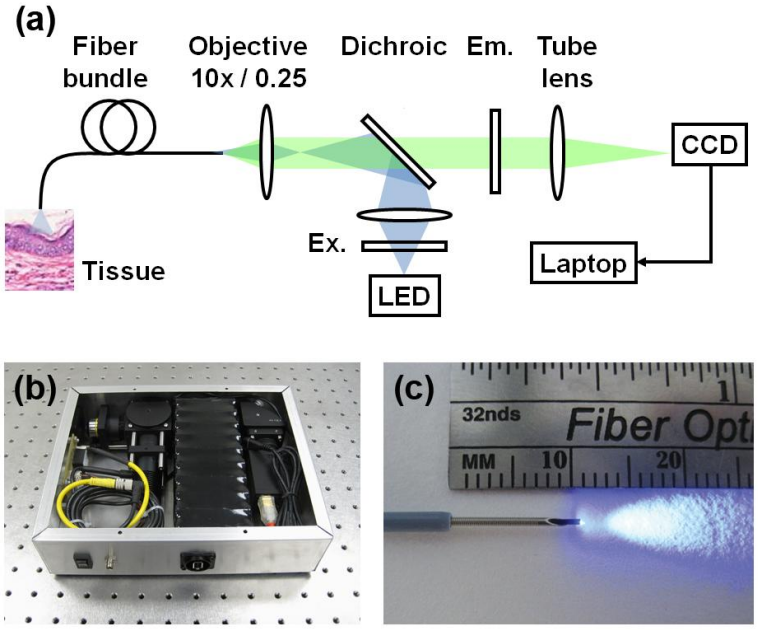

Figure 2: Representative HRME images (a,b,c) of normal, benign, and malignant lesions of the liver with corresponding photographs of H&E histopathologic sections (d,e,f). (a,d) Normal liver. Note the regularly shaped, widely and evenly spaced nuclei. (b,e) Angiomylipoma, benign lesion. Note the adipocytes with clear vacuoles. (c,f) Metastatic colon adenocarcinoma, malignant lesion. Note the loss of normal architecture with irregular glandular structures and nuclear clumping. Scale bars represent 100 µm.

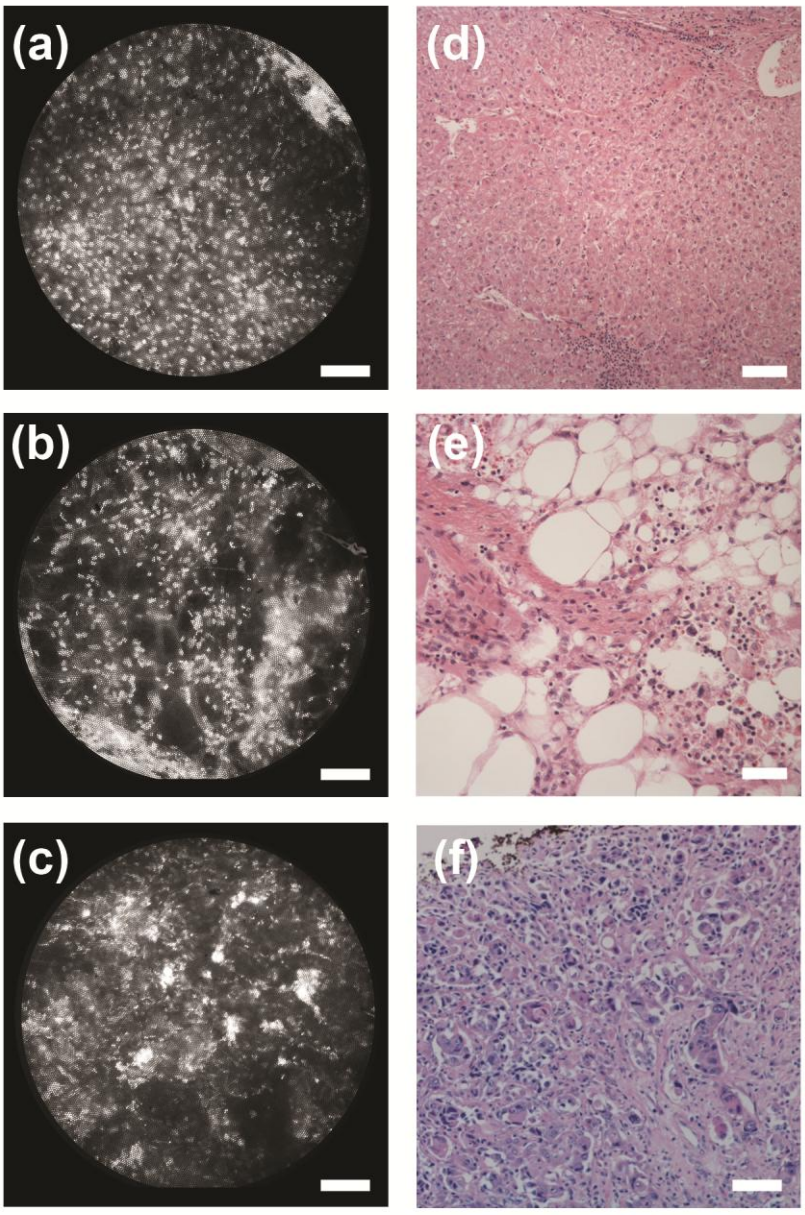

Figure 3: Representative HRME images (a,b,c) of normal, benign, and malignant lesions of the pancreas with corresponding H&E histology (d,e,f). (a,d) Normal pancreas. Note the clustering of nuclei into acinar structures. (b,e) Microcystic adenoma, benign lesion. Note the cystic spaces of varying shapes and sizes. (c,f) Ductal adenocarcinoma, malignant lesion. Note the loss of normal architecture and infiltrating poorly formed glands amidst desmoplastic stroma. Scale bars represent 100 µm.

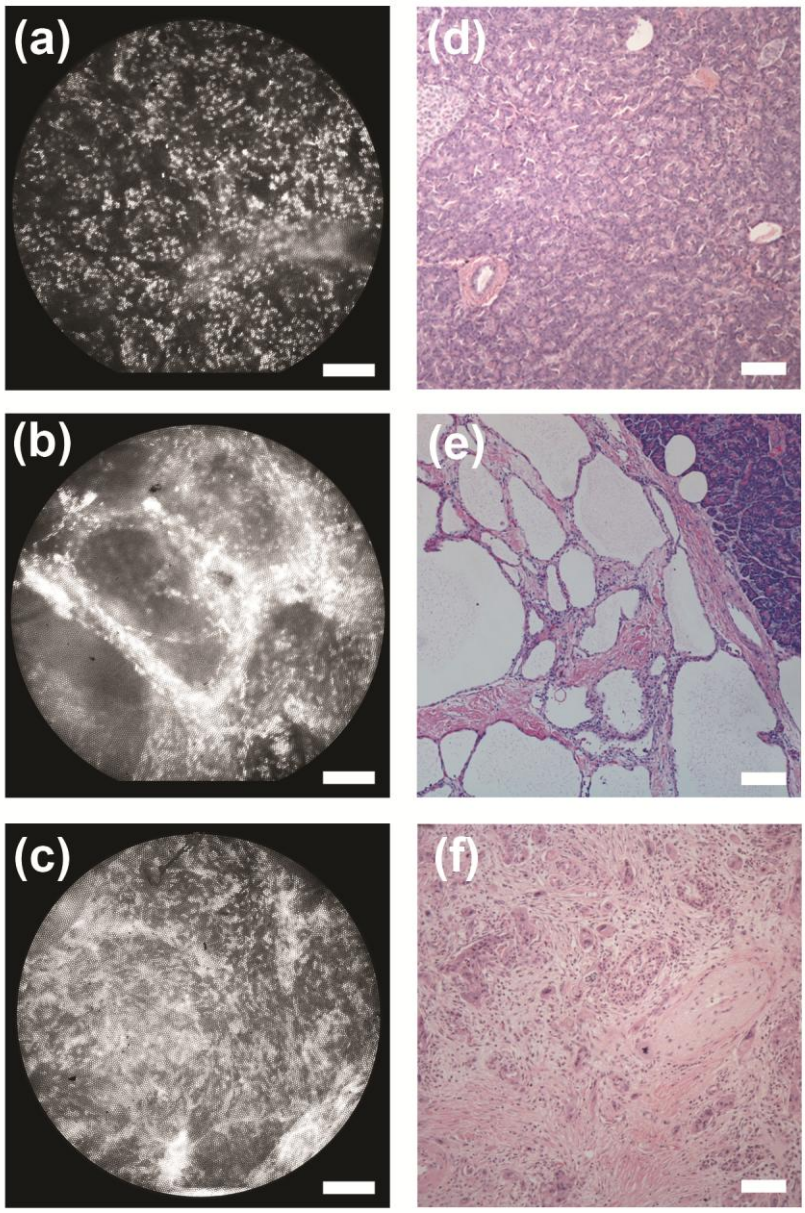

Figure 4: Representative HRME imaging of the pancreatic parenchyma in an *in vivo* swine model. Images are acquired with the fiber-optic probe advanced within the lumen of a 19-gauge EUS-FNA needle. Nuclei appear as small, discrete dots within the field of view. Scale bar represents 100 μm.

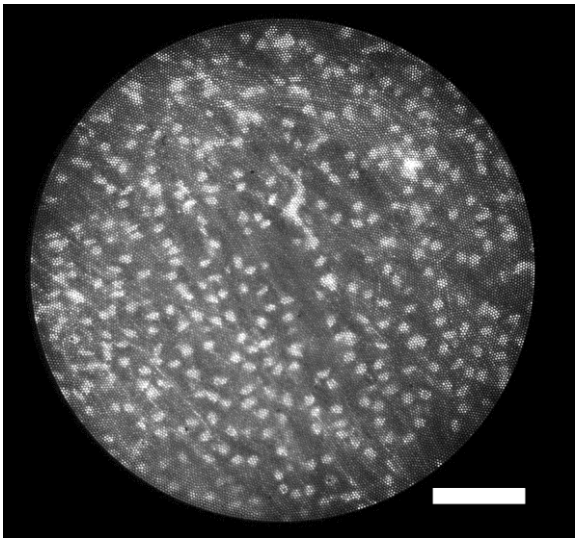

Figure 5: (a) Performance of all nine endosonographers in reading HRME image test sets. Bars represent median values. Error bars indicate the interquartile range. (b) Performance of endosonographers with no prior experience in HRME imaging ("HRME novices", n = 7) compared to endosonographers with prior experience (> 50 cases) in evaluating HRME images ("HRME experienced", n = 2). Bars represent median values. Error bars indicate the interquartile range.

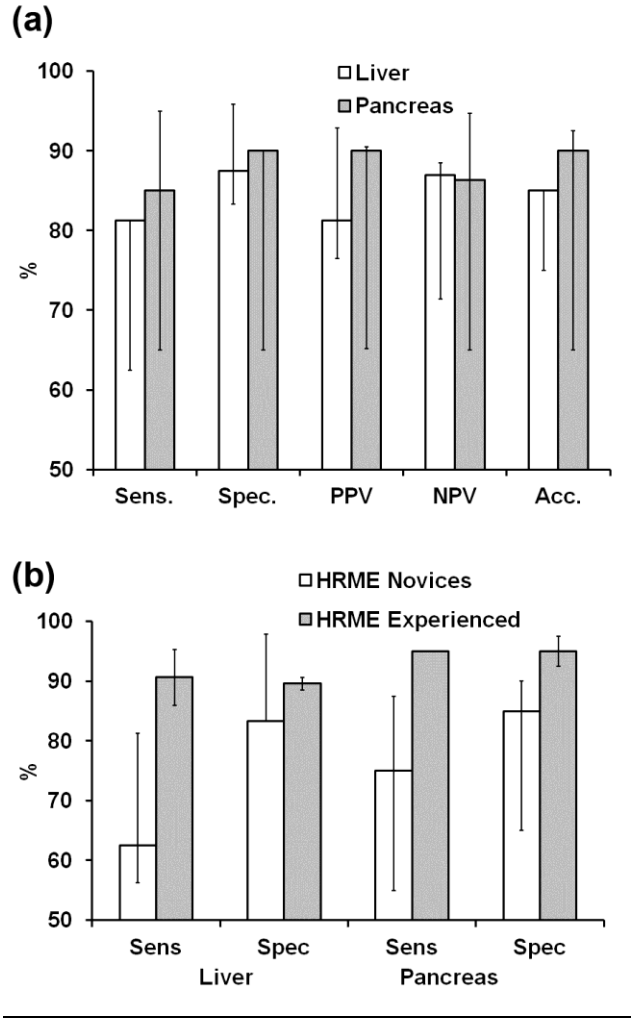

Table 1: Performance of endosonographers in recognizing normal / benign tissue from malignant in test sets of 40 HRME images for each organ. There were 24 images with pathology considered malignant for the liver test set, and 20 in the pancreas test set. HRME "experienced" endosonographers had reviewed images from over 50 HRME cases prior to this study. HRME "novices" had no prior experience in HRME imaging prior to this study. All values are percentages, rounded to the nearest whole number.

	HRME experienced		**HRME novices**							**Median**		
	1	2	1	2	3	4	5	6	7	Exp.	Nov.	All
Liver:												
Accuracy	95	85	90	63	75	83	70	85	85	90	83	85
Sensitivity	100	81	81	63	38	81	50	63	88	91	63	81
Specificity	92	88	96	63	100	83	83	100	83	90	83	88
PPV	89	81	93	53	100	77	67	100	78	85	78	82
NPV	100	88	89	71	71	87	71	80	91	94	80	87
Pancreas:												
Accuracy	93	98	65	55	90	65	68	90	93	95	68	90
Sensitivity	95	95	65	45	85	45	75	90	95	95	75	85
Specificity	90	100	65	65	95	85	60	90	90	95	85	90
PPV	91	100	65	56	94	75	65	90	91	95	75	90
NPV	95	95	65	54	86	61	71	90	95	95	71	86

References:

1. Helmstaedter L, Riemann JF, "Pancreatic cancer - EUS and early diagnosis," Langenbecks Arch Surg 2008;393:923–927.

2. Binmoeller KF, Brand B, Thul R, *et al.*, "EUS-guided, fine needle aspiration biopsy using a new mechanical scanning puncture echoendoscope," Gastrointest Endosc 1998;47:335-340.

3. Voss M, Hammel P, Molas G, *et al.*, "Value of endoscopic ultrasound guided fine needle aspiration biopsy in the diagnosis of solid pancreatic masses," Gut 2000;46:244-249.

4. Bhutani MS, Gress FG, Giovannini M, *et al.*, "The no endosonographic detection of tumor (NEST) study: a case series of pancreatic cancers missed on endoscopic ultrasonography," Endoscopy 2004;36:385-389.

5. Uehara H, Ikezawa K, Kawada N, *et al.*, "Diagnostic accuracy of endoscopic ultrasound-guided fine needle aspiration for suspected pancreatic malignancy in relation to the size of lesions," J Gastroenterol Hepatol 2011 *in press*

6. Reddy NK, Ioncică AM, Săftoiu A, *et al.*, "Contrast-enhanced endoscopic ultrasonography," World J Gastroenterol 2011;7:42-48.

7. Giovannini M, Botelberge T, Bories E, *et al.*, "Endoscopic ultrasound elastography for evaluation of lymph nodes and pancreatic masses: A multicenter study," World J Gastroenterol 2009;15;1587-1593.

8. Itokawa F, Itoi T, Sofuni A, *et al.*, "EUS elastography combined with the strain ratio of tissue elasticity for diagnosis of solid pancreatic masses," J Gastroenterol 2011 *in press*

9. Goetz M, Kiesslich R, "Advances of endomicroscopy for gastrointestinal physiology and diseases," Am J Physiol Gastrointest Liver Physiol 2010;298:G797–G806.

10. Goetz M, Deris I, Vieth M, *et al.*, "Near-infrared confocal imaging during mini-laparoscopy: A novel rigid endomicroscope with increased imaging plane depth," J Hepatol 2010;53;84-90.

11. Becker V, Wallace M, Fockens P, *et al.*, "Needle-based confocal endomicroscopy for *in vivo* histology of intraabdominal organs: First results in a porcine model," Gastrointest Endosc 2010;71:1260-1266.

12. Muldoon TJ, Pierce M, Nida DL, *et al.*, "Subcellular-resolution molecular imaging within living tissue by fiber microendoscopy," Opt Express 2007;15:16413-16423.

13. Pierce M, Yu D, Richards-Kortum R, "High-resolution fiber-optic microendoscopy for *in situ* cellular imaging," JoVE 2011;47: http://www.jove.com/index/Details.stp?ID=2306

14. Muldoon T, Anadasabapathy S, Maru D, *et al.*, "High resolution imaging in Barrett's esophagus: A novel, low cost endoscopic microscope," Gastrointest Endosc 2008;68:737-744.

15. Pierce MC, Vila PM, Polydorides AP, *et al.*, "Low-cost endomicroscopy in the esophagus and colon," Am J Gastro 2011;106:1722-1724

16. Konda VJA, Aslanian HR, Wallace MB, *et al.* First assessment of needle-based confocal laser endomicroscopy during EUS-FNA procedures of the pancreas. Gastrointest Endosc 2011;74:1049-60

17. Polglase AL, McLaren WJ, Skinner SA, *et al.*, "A fluorescence confocal endomicroscope for *in vivo* microscopy of the upper- and the lower-GI tract," Gastrointest Endosc 2005;62:686-695

18. Qiu L, Pleskow DK, Chuttani R, *et al.* Multispectral scanning during endoscopy guides biopsy of dysplasia in Barrett's esophagus. Nature Med 2010;16:603-606

19. Suter MJ, Vakoc BJ, Yachimski PS, *et al.* Comprehensive microscopy of the esophagus in human patients with optical frequency domain imaging. Gastrointest Endosc 2008;68:745-53.

20. Adler DC, Zhou C, Tsai T-H, *et al.* Three-dimensional optical coherence tomography of Barrett's esophagus and buried glands beneath neosquamous epithelium following radiofrequency ablation. Endoscopy 2009;41:773-776

21. Buchner AM, Gomez V, Heckman MG, et al. The learning curve of in vivo probe-based confocal laser endomicroscopy for prediction of colorectal neoplasia. Gastrointest Endosc 2011;73:556-560

22. Tanbakuchi, AA, Rouse AR, Udovich JA, *et al.* "Clinical confocal microlaparoscope for real-time *in vivo* optical biopsies," J Biomed Opt 14; 044030 (2009)

23. Kiesslich, R, M Goetz, A Hoffman, PR Galle, "New imaging techniques and opportunities in endoscopy," Nat Rev Gastroenterol Hepatol 2011;8:547-553